SIAM/ASA J. Uncertainty Quantification
Vol. 13, No. 4, pp. 1681–1708

Mean Field Games for Controlling Coherent Structures in Nonlinear Fluid Systems*

Yuan Gao† and Di Qi†

Abstract. This paper discusses the control of coherent structures in turbulent flows, which has broad applications among complex systems in science and technology. Mean field games have been proved a powerful tool and are proposed here to control the stochastic Lagrangian particles as players tracking the flow and tracer fields. We derive optimal control solutions for general nonlinear fluid systems using mean-field game models and develop computational algorithms to efficiently solve the resulting coupled forward and backward mean-field system. A precise link is established for the control of passive tracer density and the scalar vorticity field based on the functional Hamilton–Jacobi equations derived from the mean field models. A new iterative numerical strategy is then constructed to compute the optimal solution with fast convergence. We verify the skill of the mean-field control models and illustrate their practical efficiency on a prototype model modified from the viscous Burgers equation under various cost functions in both deterministic and stochastic formulations. The good model performance implies potential effectiveness of the strategy for more general high-dimensional turbulent systems.

Key words. mean field control, nonlinear vorticity flow, Lagrangian particles, iterative algorithm

MSC codes. 93C10, 76D55, 49M37

DOI. 10.1137/24M1632231

1. Introduction and background.

Control of complex fluid systems characterized by a wide multiscale spectrum and nonlinear coupling between different scales remains a grand challenge with crucial applications among many fields of science and engineering [6, 32, 26, 4, 16]. Flow fields undergoing turbulent motions often demonstrate large-scale coherent structures, and control of the important transporting behaviors requires dealing with the coherent structures demonstrating strong nonlinear interactions among multiple scales [35, 27, 13]. In addition, the Eulerian flow field can be captured by Lagrangian particles advected by the flow velocity. Control of key macroscopic structures in multiscale flows can be achieved through acting on the Lagrangian particles immersed in the fluid field [34, 21]. Typical examples can be found in elasticity modeling [22, 16] and fusion plasmas [14, 15], where the macroscopic fluid features can be effectively determined by controlling an electric field acting on the group motion of the microscopic polymers or charged particles. New precise theoretical analysis

*Received by the editors January 18, 2024; accepted for publication (in revised form) May 30, 2025; published electronically October 3, 2025.
https://doi.org/10.1137/24M1632231
Funding: The work of the first author was partially supported by NSF awards DMS-2204288 and DMS-2440651. The work of the second author was partially supported by ONR award N00014-24-1-2192 and NSF award DMS-2407361.

†Department of Mathematics, Purdue University, West Lafayette, IN 47907 USA (gao662@purdue.edu, qidi@purdue.edu).

and effective control strategies are still needed considering the nonlinear dynamics and high computational demand.

In recent years, mean-field game (MFG) theory was proposed independently by Lasry and Lions [28] and Huang, Malhamé, and Caines [24] to study a large game system with identical players using the dynamics of their population/distribution. The indistinguishable individual player takes strategy/control based on the population states (without observing all the strategies of other players); meanwhile the distribution of individuals yields the population dynamics. The equilibrium, also known as the Nash system, is solved by a *coupled MFG system* consisting of a forward Fokker–Planck equation (describing the evolution of the density/population of the individuals) and a backward Hamilton–Jacobi equation (HJE; describing the control/strategy of each indistinguished player); cf. [3]. Due to this simplification for large game systems, MFG has been proved to be a powerful tool to study the equilibrium behavior of infinitely many weakly interacting players [7, 12]. The associated mean-field control problem also stimulates many applications in swarm drones, generative models, transition path theory, and mathematical finance [10, 30, 19, 42].

In this paper, we propose to address the challenging problem of controlling nonlinear transport of coherent structures by developing models of MFGs. Two MFG models are introduced concerning the control of passive tracers and active Lagrangian particles under a unified formulation: First, we introduce an MFG model (3.1) for the control of *passive scalar tracers*; Second, we design a control model (3.4) for representative flow structures in the advection and diffusion of a *scalar vorticity field.* In the first tracer control model, the stochastic motion of the passive Lagrangian tracers is immersed in a prescribed fluid flow field and passively advected by the flow velocity. Thus, the tracers can be viewed as the large number of identical players in the MFGs. The dynamical behavior of the tracer density and the optimal control on each of the identical Lagrangian tracers can be solved by the corresponding MFG system with uncoupled forward and backward equations. In contrast to the passive tracers, in the flow control model, active Lagrangian particles are used as players to track the fluid vorticity field. Thus, the controlled particles become nonlocally coupled by their accumulated density function. The evolution continuum density of the particles is shown to coincide with the vorticity equation recovered by the McKean–Vlasov equation [37]. Therefore, the control of flow solutions can be inversely achieved by acting on the large number of Lagrangian particles (players). An MFG system of closely coupled forward and backward equations is derived for the optimal solution of the flow control problem. In addition, the corresponding functional HJEs are derived describing the evolution of the value function in both the tracer and flow control models. This leads to an interesting connection between the uncoupled tracer MFG system and the coupled vorticity MFG system in a unified way.

The nonlinear nature of the vorticity equation makes the corresponding Hamiltonian nonseparable and thus new decouple procedures are needed. A series of numerical strategies have been developed for solving the coupled MFG equations [2, 29]. Methods based on a fixed-point iteration [9, 23] have been used to decouple the forward and backward equations with semi-Lagrangian schemes and the Cole–Hopf transformation to convert to linear equations. One strategy, called fictitious play [8, 25], is shown to help the convergence of the fixed-point iteration using the average of the entire history of the outputs. Another approach uses the primal-dual hybrid gradient method [11, 31] to solve the control problem as a saddle point

problem. Usually, these methods require transformation of the original equations in the first step and may require a large number of iterations in numerical simulations.

Based on the typical structure of the nonlinear flow model, we propose a new strategy to efficiently find the optimal solution of the coupled MFG system without any special treatment to the original equations. The numerical method is based on the link developed for the uncoupled tracer MFG system and the coupled flow MFG equations, where the optimal solution for the coupled equations becomes a fixed point of the solution map for the uncoupled problem. This inspires an effective iterative approach by first solving the backward equation given the output solution from the previous step, then using the optimal control function to solve the density function from the forward equation. Stability and fast convergence of the proposed iterative scheme are further guaranteed by a self-adapted interpolation step during each iteration. We show the necessity of adopting this essential interpolation step to effectively reduce the cost function value in each iteration cycle. This step also is shown to enable fast convergence during the iterating updates. The model performance and the effectiveness of the proposed numerical algorithm are tested on a representative prototype model adapted from the viscous Burgers equation simulating the vortical advection by an incompressible flow field. Using the proposed iterative approach, fast convergence is observed within a few steps with efficient computation in each updating step. Performance of ensemble approximations adaptive to higher-dimensional cases are also considered.

The paper is organized as follows. A description of the tracer and flow transport equations in both deterministic and stochastic formulation is introduced in section 2. Mean field models as well as the associated systems for the control problems are constructed in section 3. The mean-field models can be written in Hamilton dynamics and a link between the tracer and flow control models is built in section 4. Effective computational schemes corresponding to the theoretical models are then proposed in section 5 with numerical confirmation on prototype models in section 6. We conclude the paper with a summarizing discussion in section 7.

2. Formulation of the fluid control equations.

We start with the basic setups and notation for the flow system and the associated control problem. In particular, the Eulerian flow system has an equivalent stochastic Lagrangian formulation based on which the MFGs will be developed.

2.1. Governing equation as the transport of the vorticity field.

Let $u(x,t)$ be the incompressible velocity field of a fluid as a function on the Eulerian spatial coordinates $x \in \mathbb{T}^d$ and time t. The fluid field can be modeled by the evolution of a *scalar vorticity field* $q(x,t)$ according to the standard advection-diffusion equation

$$\frac{\partial q}{\partial t} + u \cdot \nabla q = D(\Delta) q + f(x,t), \quad u(x,t) = \mathcal{T} q(x,t), \quad q(x,0) = q_0(x). \tag{2.1}$$

On the right-hand side of the equation, the flow is subject to an external forcing effect represented by $f(x,t)$ and generalized damping and dissipation effects $D(\Delta)$. The velocity field satisfies $\nabla \cdot u = 0$ due to incompressibility. Therefore, the vorticity field $q(x,t)$ is uniquely linked to the velocity field by the (invertible) linear operator, $u = \mathcal{T} q$, so that the flow solution is fully represented by the scalar vorticity transported by the flow velocity. The scalar model can serve as a desirable general framework for developing theories and practical methods for turbulent transport and control of coherent structures [33, 38]. Applications of the

general fluid advection-diffusion model (2.1) include wide classes of turbulent flows in realistic natural and engineering systems such as the passive tracer diffusion [34], turbulent transport in geophysical turbulence [38, 39], and anomalous transport in fusion plasmas [15, 41].

It is noticed that the above equation (2.1) usually permits a set of metastable steady state solutions [40]. The steady states provide a natural characterization of the coherent structures observed in the flow field, while multiscale turbulent features are usually developed in the solution of the vorticity flow (2.1). We will design two mean-field control models based on the complex fluid structures generated in the vorticity equation (2.1). First, in the control of the passive tracer field, the solution of (2.1) provides the (known) background advection flow that transports the passive tracers. Second, in considering the control of the flow field, we design the additional "control forcing" that transforms the key coherent structures in the flow field. Our attention will be given to finding the optimal transition undergoing some transient motions from one initial state to another final steady state by imposing a proper external forcing effect in either the tracer density or the flow vorticity field.

Remark 2.1. One motivating example of (2.1) comes from the two-dimensional turbulence, where the potential vorticity $q = Z(\psi)$ is associated with the flow stream function ψ via a linear operator Z and may include a variety of physical effects (for example, $Z(\psi) = \Delta\psi$). Then the corresponding velocity field can be determined by the stream function as $u = \nabla^{\perp}\psi = (-\partial_y\psi, \partial_x\psi)$ through a linear operator.

2.2. Stochastic Lagrangian equations for particle transport. From a stochastic perspective, the continuity equation of the flow field (2.1) can be captured by the collective performance of a group of *Lagrangian particles* X_s transported by the flow velocity field. In addition, we introduce a *control field* α_s as the additional driving force exerted on the flow or tracer field. In the mean-field game context, those particles are also called indistinguished individual players.

We introduce the fluid state (i.e., the population/vorticity) from the solution of the vorticity equation (2.1) as $q_s(\cdot), t \le s \le T$. The velocity field is then denoted as $u_s(x; q_s) = \mathcal{T} q_s(x)$ explicitly indicating the direct relation with q_s. Suppose for now that the control field $\alpha_s(x; q_s)$ is given dependent on the fluid motion, which will be determined by an optimization procedure as described next in section 3. Then the trajectory of each of the particles is described by the stochastic differential equation (SDE)

$$\mathrm{d}X_s = [u_s(X_s; q_s) + \alpha_s(X_s; q_s)]\,\mathrm{d}s + \sqrt{2D}\mathrm{d}W_s, \quad t \le s \le T, \quad X_t \sim \rho_t(x). \tag{2.2}$$

Here $u_s(\cdot; q_s), \alpha_s(\cdot; q_s)$ indicate the possible dependence on the fluid field $\{q_s\}_{t \le s \le T}$ for the transport velocity and the control. The molecular diffusion effect is represented by Gaussian white noise with a diffusivity coefficient D. First in the tracer control problem, we seek to describe the probability measure, describing the law of individuals $X_s \sim \rho_s(x)$. With the given flow velocity u_s, the governing equation will satisfy the Kolmogorov forward equation for the SDE (2.2),

$$\partial_s \rho_s(x) + \nabla \cdot [(u_s(x; q_s) + \alpha_s(x; q_s))\,\rho_s(x)] = D\Delta\rho_s(x), \quad t \le s \le T, \tag{2.3}$$

with the initial condition from the initial tracer configuration in the fluid field, $X_t \sim \rho_t(x)$. Notice that given a fluid vorticity state q_s, the law of individuals ρ_s does not necessary coincide

with q_s (that is, the controlled tracer density field may not exactly track the evolution of the vorticity flow).

Next, treating the fluid vorticity q_s as an unknown state to be optimized, we control the vorticity equation (2.1) by introducing an external forcing in the form

$$f(x,s) = -\nabla \cdot [\alpha_s(x)\, q_s(x)], \tag{2.4}$$

according to the same control effect α_s in the SDE formulation (2.2). The special form of control forcing in (2.4) acts as an additional action in the form of a transport term to move the flow particles to the target configuration. The resulting flow equation becomes

$$\partial_s q_s(x) + \nabla \cdot [(u_s(x;q_s) + \alpha_s(x;q_s))\, q_s(x)] = D\Delta q_s(x), \quad t \le s \le T, \tag{2.5}$$

exploiting the divergence-free velocity field, $\nabla \cdot u_s = 0$. Notice that the vorticity field q_s is not passively advected by the fluid field and actually determines the velocity field u_s. Nevertheless, in the control problems discussed next, we can view the field q_s as *a proper measure* on the state space since it is solved by the continuity equation (2.3) up to a constant normalization constant. In particular, if we set the initial condition $q_t = \rho_t$ in (2.2), the flow vorticity field q_s will take the same form as the tracer density measure generated by the stochastic samples advected by the velocity field $u_s(x;q_s)$. The equivalence between the controlled flow equation (2.5) and the SDE for an ensemble of particles implies the possibility to control the key flow structures by acting on the measurements of Lagrangian particles.

3. Control of the fluid fields with mean-field games.

Here, we propose the control models for the transport of both the tracer density and the fluid vorticity fields. We first formulate the problems based on the PDEs. Then, the corresponding stochastic control for the Lagrangian particles can be formulated in an equivalent way.

3.1. Control of the tracer density field with a given fluid solution.

First, we propose a mean-field game model (MFG-1) concerning *a mean-field game for indistinguished individuals* with a given fluid dynamics. Given the flow vorticity solution $q_s(x), t \le s \le T$, consider the optimal control problem about the value function on the optimal solutions $\rho(\cdot) := \rho_s(x), \alpha(\cdot) := \alpha_s(x), s \in [t,T], x \in \mathbb{T}^d$,

$$\begin{aligned} \mathcal{U}(\rho,t) := \inf_{\rho(\cdot),\alpha(\cdot)} \left(\int G(x,q_T)\rho_T(x)\,\mathrm{d}x + \int_t^T \left\{ \int [L(\alpha_s) + F(x,q_s)]\rho_s(x)\,\mathrm{d}x \right\} \mathrm{d}s \right), \\ \text{s.t. } \partial_s \rho_s + \nabla \cdot [(\mathcal{T} q_s + \alpha_s)\rho_s] = D\Delta\rho_s, \quad t \le s \le T, \quad \text{and } \rho_t(x) = \rho(x), \end{aligned} \tag{3.1}$$

where we denote the terms to be optimized under inf as $\mathcal{J}(\rho(\cdot),\alpha(\cdot))$. Here, the *running cost* $L(\alpha)$ depends on the individual control action; the *individual running cost* $F(x,q)$ represents the running cost interacting with the fluid field; and the *terminal cost* $G(x,q)$ depends on the final flow state. The dependence on the fluid field can be either global or local, and we will describe the specific forms of these functionals in section 5.1. Here, the solution ρ_s of the continuity equation in (3.1) can be viewed as the density field of the controlled tracers (2.2), driven by the velocity field u_s generated from the given flow vorticity solution q_s. We will refer to the optimization problem (3.1) as the MFG-1 model. The solution of the MFG-1

model describes the optimal control of the tracer density from the initial configuration ρ to the final target ρ_T.

The optimal solution of the MFG-1 model given a fixed flow vorticity solution q_s is described by the following proposition for the corresponding Euler–Lagrange equations.

Proposition 3.1. *Given the flow vorticity field $q_s(x), s \in [t,T]$, the optimal tracer density $\rho_s(x)$ under the cost function (3.1) with $L(\alpha) = \frac{1}{2}|\alpha|^2$ is given by the solution of the following MFG-1 system:*

$$\partial_s \rho_s + \nabla \cdot [(\mathcal{T} q_s + \nabla \phi_s)\, \rho_s] = D\Delta \rho_s, \ \ t \le s \le T,\ \rho_t(x) = \rho(x), \tag{3.2a}$$

$$\partial_s \phi_s + \frac{1}{2}|\nabla \phi_s|^2 + \nabla \phi_s \cdot \mathcal{T} q_s + D\Delta \phi_s = F(x, q_s), \ \ t \le s \le T,\ \phi_T(x) = -G(x, q_T). \tag{3.2b}$$

The corresponding optimal control can be solved by $\alpha_s(x) = \nabla \phi_s(x)$.

Thus, we have a decoupled MFG system (3.2) for the MFG-1 model. The proof of Proposition 3.1 can be found in the supplementary materials (supplement_mfg.pdf [local/web 1.78MB]).

3.2. Control of the vorticity flow field as a potential mean-field game. Next, we design the control of the vorticity flow stated in (2.1) as an MFG system. In particular, we are seeking the control forcing in the specific form as (2.4), where α_s is the additional control vector that aims to drive the initial flow state to the final target. Combining with the original vorticity equation (2.1), we find the control PDE associated with the control forcing as

$$\partial_s q_s + \nabla \cdot [(\mathcal{T} q_s + \alpha_s)\, q_s] = D\Delta q_s, \quad t \le s \le T, \tag{3.3}$$

with the prescribed initial state $q\ |_{s=t} = q(x)$. The equation describes the control of the vorticity flow field q_s from the initial state q at $s = t$ to a final target field q_T at $s = T$ through the control α_s. Notice that this flow control equation is different from the tracer control equation (2.3) because the controlled vorticity is to be optimized with the nonlinear coupling, in contrast to the prescribed velocity field in (2.3). Even though it may seem impractical to control the entire flow field, the control equation (3.3) provides mathematical guidance for designing effective forcing α_s acting on colloids of particles in complex fluids such as the control of surfactant chemicals [22], charged particles [14], and ionic soft matter [16].

Here, we propose the potential mean-field game model (MFG-2) concerning the control of the fluid vorticity field. Instead of controlling the tracer density field ρ_s advected by the flow field, we consider the direct optimal control of the flow vorticity state, that is,

$$\begin{aligned} \mathcal{V}(q,t) := \inf_{q(\cdot),\alpha(\cdot)} & \left(\mathcal{G}(q_T) + \int_t^T \left[\int L(\alpha_s)\, q_s(x)\, \mathrm{d}x + \mathcal{F}(q_s) \right] \mathrm{d}s \right), \\ \text{s.t.}\ \ & \partial_s q_s + \nabla \cdot [(\mathcal{T} q_s + \alpha_s)\, q_s] = D\Delta q_s, \quad t \le s \le T, \quad \text{and } q_t(x) = q(x), \end{aligned} \tag{3.4}$$

where we denote the terms under inf as $\mathcal{I}(q(\cdot), \alpha(\cdot))$. We will refer to the optimization problem (3.4) as the MFG-2 model. In the above potential game model, we assume that the running cost $\mathcal{F}$ and the terminal cost $\mathcal{G}$ satisfy $F(x,q) = \frac{\delta \mathcal{F}}{\delta q}(q,x)$, $G(x,q) = \frac{\delta \mathcal{G}}{\delta q}(q,x)$, as a connection to the MFG-1 model (3.1). In contrast to the MFG-1 model (3.1), the flow vorticity q_s becomes

the controlled state in the MFG-2 model rather than the tracer density ρ_s. This leads to the nonlinear continuity equation in (3.4).

Still, we can solve the optimization problem by deriving the Euler–Lagrangian equations. The following proposition provides the Euler–Lagrangian equations for the optimal solution of the MFG-2 model.

Proposition 3.2. *The optimally controlled flow solution in MFG-2 model (3.4) with* $L(\alpha) = \frac{1}{2}|\alpha|^2$ *is given by* q_s *and the associated optimal control for the flow field is given by* $\alpha_s = \nabla\varphi_s$, *where* $(q_s, \varphi_s), s \in [t, T]$ *solves the following MFG-2 system:*

$$\partial_s q_s + \nabla \cdot [(\mathcal{T} q_s + \nabla\varphi_s) q_s] = D\Delta q_s, \quad t \le s \le T, \tag{3.5a}$$
$$q_t(x) = q(x),$$

$$\partial_s \varphi_s + \frac{1}{2}|\nabla\varphi_s|^2 + \nabla\varphi_s \cdot \mathcal{T} q_s + \mathcal{T}^* \cdot (\nabla\varphi_s q_s) + D\Delta\varphi_s = F(x, q_s), \quad t \le s \le T, \tag{3.5b}$$
$$\varphi_T(x) = -G(x, q_T).$$

The proof of Proposition 3.2 can be found in the supplementary materials (supplement_mfg.pdf [local/web 1.78MB]).

3.3. SDE formulations for the mean-field game models. From a different perspective, we can reformulate the above PDE models for controlling tracer density and fluid vorticity as SDEs representing particles in Lagrangian form. The SDE formulation can also help to propose effective computational strategies based on simulation of the stochastic samples.

First, the continuity equation in the MFG-1 model (3.1) can be viewed as the density equation of the motion of the stochastic particles (2.2). Therefore, we can formulate the following stochastic optimal control problem (referred to as the MFG-1′ model) for the corresponding stochastic control problem with the given flow solution $q_s(x), t \le s \le T$:

$$\mathcal{U}(\rho, t) := \inf_{\rho(\cdot), \alpha(\cdot)} \mathbb{E}\left\{ G(X_T, q_T) + \int_t^T [L(\alpha_s(X_s)) + F(X_s, q_s)] \mathrm{d}s \right\}, \tag{3.6}$$
$$\text{s.t. } \mathrm{d}X_s = [\mathcal{T} q_s(X_s) + \alpha_s(X_s)]\,\mathrm{d}s + \sqrt{2D}\mathrm{d}W_s, \quad t \le s \le T, \text{ and } X_t \sim \rho(x).$$

The optimal solution of the MFG-1′ model can still be solved by the Euler–Lagrangian equations using the equivalent representation (3.2) in the Eulerian problem, so that we have the following corollary.

Corollary 3.3. *With the flow vorticity field* $q_s, s \in [t, T]$ *given, the solution* (ρ_s, ϕ_s) *of the MFG-1 system (3.2) provides the optimal solution of the stochastic MFG-1′ model (3.6).*

Then, the control forcing (2.4) can be viewed as the additional drifting effect α_s that is externally exerted on the local particles, which in an optimal way is given by $\alpha_s = \nabla\varphi_s$. We can introduce the McKean–Vlasov equation

$$\mathrm{d}X_s = [u_s(X_s; \rho_s) + \alpha_s(X_s; \rho_s)]\,\mathrm{d}s + \sqrt{2D}\mathrm{d}W_s.$$

The tracer density as the law of the above stochastic particle $X_s \sim \rho_s$ is solved by the continuity equation in the form

$$\partial_s \rho_s + \nabla \cdot [(u_s + \alpha_s)\rho_s] = D\Delta\rho_s.$$

Let q_s be a solution of the controlled flow vorticity equation (3.3). With the same form of α_s and $u_s = \mathcal{T} q_s$, we have $\rho_s = q_s$ due to the uniqueness for linear equations.

Similarly, according to the MFG-2 model (3.4), we give the following stochastic control problem as the expectation with respect to q_s (referred to as the MFG-2′ model):

$$\begin{aligned} \mathcal{V}(q,t) := \inf_{q(\cdot),\alpha(\cdot)} \mathbb{E}\left\{ \tilde{G}(X_T, q_T) + \int_t^T \left[L\left(\alpha_s\left(X_s\right)\right) + \tilde{F}\left(X_s, q_s\right) \right] \mathrm{d}s \right\}, \\ \text{s.t. } \mathrm{d}X_s = \left[\mathcal{T} q_s\left(X_s\right) + \alpha_s\left(X_s\right) \right] \mathrm{d}s + \sqrt{2D}\mathrm{d}W_s, \quad t \le s \le T, \text{ and } X_t \sim q(x). \end{aligned} \tag{3.7}$$

Above, q_s is acting as the law of the random particles X_s in the nonlinear field. In contrast to the density control problem in (3.6) with a given velocity field, q_s will also be optimized together with the control. The initial sample is drawn from the initial flow state $X_t \sim q$. Still, we assume the MFG-2 model (3.4) is a potential game with the cost functionals $\mathcal{F}, \mathcal{G}$ satisfying

$$\mathcal{F}(q) = \int \tilde{F}(x,q)\, q(x) \mathrm{d}x, \quad \mathcal{G}(q) = \int \tilde{G}(x,q)\, q(x) \mathrm{d}x.$$

Notice that the new costs $\tilde{F}, \tilde{G}$ may not necessarily be the same as the F, G in (3.6). In a similar way, the solution of the MFG-2′ model is given by the same Euler–Lagrangian equations in (3.5).

Corollary 3.4. *With the same initial law $q = \rho$, the solution (ρ_s, φ_s) of MFG-2 system (3.5) provides an optimal solution of the stochastic MFG-2′ model (3.7).*

Mean field game with finite number of players. The empirical distribution of a group of N particles is supposed to recover the global vorticity field

$$q_s^N(x) = \frac{1}{N} \sum_{i=1}^N \delta_{X_s^i}(x) \cong q_s(x), \tag{3.8}$$

as $N \to \infty$. If the control velocity field α for SDE (2.2) and for (3.3) coincide, the continuity PDE (3.3) becomes the Kolmogorov forward equation for the SDE (2.2) for particles, thus q_s plays the equivalent role of a probability density measure that uniformly describes the statistics of all the particle trajectories $\{X_s^i\}$. Notice that the control α_s depends on the entire density q_s, thus finding the optimal control finally leads to an MFG problem.

We can find the associated stochastic differential game with mean-field interaction based on the SDE model (2.2) using the proposed cost functionals in (3.4),

$$\begin{aligned} \mathcal{V}^N(q,t) := \inf_{q^N(\cdot),\alpha^N(\cdot)} \mathbb{E}\left\{ \tilde{G}\left(X_T^i, q_T^N\right) + \int_t^T \left[L\left(\alpha_s^N\left(X_s^i\right)\right) + \tilde{F}\left(X_s^i, q_s^N\right) \right] \mathrm{d}s \right\}, \\ \text{s.t. } \mathrm{d}X_s^i = \left[\mathcal{T} q_s^N\left(X_s^i\right) + \alpha_s^N\left(X_s^i\right) \right] \mathrm{d}s + \sqrt{2D}\mathrm{d}W_s^i, \quad t \le s \le T,\ X_t^i \sim q, \end{aligned} \tag{3.9}$$

for samples $i = 1, \ldots, N$. Above, q_s^N is the empirical distribution (3.8) of the group of finite players $\{X_s^i\}_{i=1}^N$, and α_s^N is implicitly dependent on the empirical distribution of the N samples. The advantage of using this finite particle model (3.9) is that we are able to find

the optimal control for the complex flow field by controlling the finite number of Lagrangian tracers. This enables an efficient Monte Carlo (MC) type approach to capture the continuous fluid solution. We refer to [28] for the mean-field limit from the above stochastic differential game with mean-field interaction to the mean-field game system in the central planer form. We will also test this finite ensemble model in the numerical tests in section 6.2.2.

4. Functional Hamilton–Jacobi equations for the value functions. In this section, we demonstrate that the MFG models in (3.2) and (3.5) can be recast in Hamiltonian forms. Thus the value functions $\mathcal{U}(\rho,t)$ and $\mathcal{V}(\rho,t)$ satisfy the corresponding functional HJEs. Under the functional HJE formulations, the coupled MFG-2 model can be shown to be related to a modified MFG-1 model with given optimal solutions.

4.1. Functional HJE for the MFG-1 model. First, the MFG-1 model (3.1) for controlling tracer density transport has the Hamiltonian functional

$$\mathcal{H}_1(\rho,\phi;q)=\int\left[\frac{1}{2}|\nabla\phi|^2+\nabla\phi\cdot\mathcal{T}q(x)+D\Delta\phi-F(x,q)\right]\rho(x)\,\mathrm{d}x \tag{4.1}$$

with $q(x)$ the solution of the prescribed flow vorticity field. It can be found that the Euler–Lagrangian equations (3.2) follow the Hamilton dynamics for $s\in[t,T]$,

$$\partial_s\rho_s=\frac{\delta\mathcal{H}_1}{\delta\phi}(\rho_s,\phi_s;q_s),\qquad \partial_s\phi_s=-\frac{\delta\mathcal{H}_1}{\delta\rho}(\rho_s,\phi_s;q_s) \tag{4.2}$$

with $\rho_t=\rho$, and q_s given by the background advection flow solution. In particular, since $q(x)$ is given we can define the local Hamiltonian function H_1 according to the separable Hamiltonian functional (4.1) as

$$H_1(x,p;q)=\frac{1}{2}|p|^2+\mathcal{T}q(x)\cdot p, \tag{4.3}$$

and the corresponding Lagrangian becomes

$$L(x,b;q)=\sup_p\{b\cdot p-H_1(x,p;q)\}=\frac{1}{2}|b-\mathcal{T}q(x)|^2,$$

and with the convexity the supremum is reached at $p^*=b-\mathcal{T}q(x)$. Thus, the Lagrangian functional can be redefined as $L(x,\alpha;q):=L(x,b(x,\alpha);q)=\frac{1}{2}|\alpha|^2$. The Hamiltonian functional (4.1) can be represented by the local Hamiltonian (4.3) as

$$\mathcal{H}_1(\rho,\phi;q)=\int\left[H_1(x,\nabla\phi;q)+D\Delta\phi-F(x,q)\right]\rho(x)\,\mathrm{d}x.$$

And we can introduce the optimal "total velocity" as $b_s(x)=\partial_pH_1(x,\nabla\phi_s;q_s)=\mathcal{T}q_s(x)+\nabla\phi_s$.

Since the MFG-1 system (3.2) is decoupled, we can directly compute the value function and its relation with the HJE solution ϕ_s, $t\le s\le T$. Let $\mathcal{U}(\rho,t;q)$ be the optimal value function from the MFG-1 model (3.1) with the given flow solution $q_t=q$. The following proposition gives the functional HJE for the MFG-1 model.

Proposition 4.1. *Given a fluid vorticity field* $\{q_s\}_{t\le s\le T}$, *let* $\mathcal{U}(\rho,t;q(\cdot))$ *be the optimal value function of the MFG-1 model* (3.1), *whose minimizer is the classical solution* (ρ_s,ϕ_s) *to the MFG system* (3.2). *Then we have* $\phi_t=-\frac{\delta\mathcal{U}}{\delta\rho}(\rho_t,x,t;q(\cdot))$ *for any* $t\le T$ *and the value function satisfies the functional HJE*

$$\begin{aligned}&\partial_t\mathcal{U}(\rho,t;q(\cdot))-\mathcal{H}_1\left(\rho,-\frac{\delta\mathcal{U}}{\delta\rho}(\rho,x,t;q(\cdot));q_t\right)=0\quad\forall t\le T,\\&\mathcal{U}(\rho,T;q(\cdot))=\int G(x,q_T)\rho(x)\,\mathrm{d}x.\end{aligned}\tag{4.4}$$

In the above, given a fluid vorticity field $q(\cdot):=\{q_s\}_{t\le s\le T}$, we denote $\mathcal{U}(\rho,t;q(\cdot)):=\mathcal{U}(\rho,t;\{q_s\}_{t\le s\le T})$ to indicate that the dependence of $\mathcal{U}$ on $q(\cdot)$ is in terms of the whole given curve, while the dependence of $\mathcal{U}$ on ρ is only in terms of the initial state $\rho_t=\rho$. The proof of Proposition 4.1 is given in the supplementary materials (supplement_mfg.pdf [local/web 1.78MB]).

4.2. Functional HJE for the MFG-2 model. Similar to the last subsection, the Hamiltonian functional for the MFG-2 model (3.4) can be found as

$$\mathcal{H}_2(q,\varphi)=\int\left[\left(\frac{1}{2}|\nabla\varphi|^2+\nabla\varphi\cdot\mathcal{T}q\right)q(x)-D\nabla\varphi\cdot\nabla q\right]\mathrm{d}x-\mathcal{F}(q).\tag{4.5}$$

The following Hamiltonian system is still valid for the MFG-2 model (3.5):

$$\partial_s q_s=\frac{\delta\mathcal{H}_2}{\delta\varphi}(q_s,\varphi_s),\qquad\partial_s\varphi_s=-\frac{\delta\mathcal{H}_2}{\delta q}(q_s,\varphi_s).\tag{4.6}$$

We can also use the local Hamiltonian function to express the functional Hamiltonian

$$\begin{aligned}&H_2(x,p,q)=\frac{1}{2}|p|^2+\mathcal{T}q\cdot p,\\&\mathcal{H}_2(q,\varphi)=\int\left[H_2(x,\nabla\varphi(x),q)\,q(x)-D\nabla\varphi\cdot\nabla q\right]\mathrm{d}x-\mathcal{F}(q).\end{aligned}\tag{4.7}$$

Above, we have $H_2(x,p,q)=\sup_\alpha\{b(q,\alpha)\cdot p-L(\alpha)\}=\sup_\alpha\{(\mathcal{T}q+\alpha)\cdot p-\frac{1}{2}|\alpha|^2\}$ with the optimal $\alpha^*=p$. The optimal total velocity is defined in the same way as $b_s(x)=\partial_pH_2(q_s(x),\nabla\varphi_s(x))=\mathcal{T}q_s(x)+\nabla\varphi_s(x)$. Notice that compared with (4.2) the Hamiltonian functional (4.7) becomes nonseparable, i.e., $H_2(x,p,q)$ is not in the form of $f_1(x,p)+f_2(x,q)$ [18]. This nonseparable Hamiltonian comes from the nature of the original nonlinear fluid drift.

We have the following proposition for the value function of the MFG-2 model.

Proposition 4.2. *Assume the MFG-2 model* (3.4) *achieves an optimal solution* $(\rho_s,\phi_s)_{t\le s\le T}$, *which solves MFG-2 system* (3.5). *Then the optimal value function* $\mathcal{V}(q,t)$ *in the MFG-2 model* (3.4) *is the solution to the following functional HJE:*

$$\partial_t\mathcal{V}(q,t)-\mathcal{H}_2\left(q,-\frac{\delta\mathcal{V}}{\delta q}\right)=0\ \forall t\le T;\quad\mathcal{V}(q,T)=\mathcal{G}(q).\tag{4.8}$$

In detail, for the MFG-2 model we have

$$\partial_t \mathcal{V}(q,t) - \frac{1}{2}\int \left|\nabla \frac{\delta \mathcal{V}}{\delta q}(q,x,t)\right|^2 q(x)\,\mathrm{d}x + \int \left(\nabla \frac{\delta \mathcal{V}}{\delta q}(q,x,t)\cdot \mathcal{T}q(x)\right) q(x)\,\mathrm{d}x$$
$$- D\int \nabla \frac{\delta \mathcal{V}}{\delta q}(q,x,t)\cdot \nabla q(x)\,\mathrm{d}x + \mathcal{F}(q) = 0, \quad t \le T.$$

In addition, the control solution $\partial_s \varphi_s = -\frac{\delta \mathcal{H}_2}{\delta q}(q_s,\varphi_s)$ *satisfies* $\varphi_s(x) = -\frac{\delta \mathcal{V}}{\delta q}(q_s,x,s)$.

The proof of Proposition 4.2 is essentially in parallel with the proofs in [20, 7] according to Hamilton system (4.6) and can be found in the supplementary materials (supplement_mfg.pdf [local/web 1.78MB]).

4.3. Link between the MFG-1 and MFG-2 models. From the previous discussions, we find that the MFG-1 model (3.1) gives decoupled equations for ρ_s and ϕ_s, especially with the linear continuity equation (3.2a) given the flow and control fields q_s and ϕ_s. On the other hand, the MFG-2 model (3.4) leads to closely coupled forward and backward nonlinear equations, which require additional efforts for strategies to effectively solve the optimal functions. Here, we establish a link between the two models, such that the MFG-2 model can be approached by an approximated form of the MFG-1 model. This enables the effective computational strategy that will be discussed next in section 5.

In order to develop a decoupled approximate model, we introduce the functional Hamiltonian on the functions $(\tilde{q},\tilde{\phi})$ based on some given solutions (q,φ),

$$\tilde{\mathcal{H}}_2\left(\tilde{q},\tilde{\phi};q,\varphi\right) = \int \left[\left(\frac{1}{2}\left|\nabla\tilde{\phi}\right|^2 + \mathcal{T}q\cdot\nabla\tilde{\phi} + D\Delta\tilde{\phi}\right)\tilde{q} + \left(q\nabla\varphi\cdot\mathcal{T}\tilde{q} - F(x,q)\,\tilde{q}\right)\right]\mathrm{d}x. \tag{4.9}$$

Comparing with the Hamiltonian (4.5), we modify the coupling term, $(\nabla\varphi\cdot\mathcal{T}q)q$, into two separable components, $(\nabla\varphi\cdot\mathcal{T}\tilde{q})q$ and $(\nabla\tilde{\phi}\cdot\mathcal{T}q)\tilde{q}$. The running cost $\mathcal{F}(q)$ is also replaced by the separable one, $\int F(x,q)\tilde{q}$. Therefore, this new Hamiltonian functional $\tilde{\mathcal{H}}_2$ fits into the MFG-1 model (4.1) with a modified running cost function

$$\tilde{F}(x,q,\varphi) = F(x,q) - \mathcal{T}^*\cdot(q\nabla\varphi).$$

The new Hamiltonian functional (4.9) leads to the following decoupled forward and backward equations:

$$\partial_s\tilde{q}_s = \frac{\delta\tilde{\mathcal{H}}_2}{\delta\tilde{\phi}}\left(\tilde{q}_s,\tilde{\phi}_s;q_s,\varphi_s\right) = -\nabla\cdot\left[\left(\mathcal{T}q_s + \nabla\tilde{\phi}_s\right)\tilde{q}_s\right] + D\Delta\tilde{q}_s, \tag{4.10a}$$

$$\partial_s\tilde{\phi}_s = -\frac{\delta\tilde{\mathcal{H}}_2}{\delta\tilde{q}}\left(\tilde{q}_s,\tilde{\phi}_s;q_s,\varphi_s\right) = -\frac{1}{2}\left|\nabla\tilde{\phi}_s\right|^2 - \mathcal{T}q_s\cdot\nabla\tilde{\phi}_s - D\Delta\tilde{\phi}_s + \tilde{F}(x,q_s,\varphi_s) \tag{4.10b}$$

with initial condition $\tilde{q}_t(x) = \tilde{q}(x)$ and final condition $\tilde{\phi}_T(x) = -G(x,q_T)$. Notice that the equations (4.10) agree with the MFG-1 model (3.2) using the new running cost function $\tilde{F}$. Therefore, using Proposition 3.1 the solutions $(\tilde{q}_s,\tilde{\phi}_s), t \le s \le T$, to (4.10) solve the corresponding optimization problem as a *modified MFG-1 model,*

$$\inf_{\tilde{q}(\cdot),\tilde{\alpha}(\cdot)}\left(\int G(x,q_T)\tilde{q}_T(x)\,\mathrm{d}x + \int_t^T\left\{\int\left[L(\tilde{\alpha}_s) + \tilde{F}(x,q_s,\alpha_s)\right]\tilde{q}_s(x)\,\mathrm{d}x\right\}\mathrm{d}s\right), \tag{4.11}$$
$$\text{s.t.}\quad \partial_s\tilde{q}_s + \nabla\cdot\left[\left(\mathcal{T}q_s + \tilde{\alpha}_s\right)\tilde{q}_s\right] = D\Delta\tilde{q}_s, \quad t\le s\le T, \quad \text{and } \tilde{q}_t = \tilde{q},$$

conditional on the given functions (q_s, φ_s) with $\alpha_s = \nabla\varphi_s$. Here, we simply use $\tilde{F}(x,q,\alpha)$ to represent $\tilde{F}(x,q,\varphi)$ when $\alpha = \nabla\varphi$. More important, if we can find the optimal solution such that $\tilde{q}_s = q_s, \tilde{\alpha}_s = \alpha_s$, the optimal solution of (4.10) gives the solution to the MFG-2 model (3.5). This implies that we may seek the optimal solution for the coupled MFG-2 model (3.5) through the solutions from the above decoupled MFG-1 model (4.11) as a fixed-point problem.

Next, if we take the function φ_s from the solutions of the MFG-2 model (3.5b) according to any solution of q_s, this gives the optimal value function based on (4.11),

$$\tilde{\mathcal{U}}\left(\tilde{q}, t; q\left(\cdot\right)\right) = \inf_{\tilde{q}(\cdot),\tilde{\alpha}(\cdot)} \mathcal{J}\left(\tilde{q}\left(\cdot\right), \tilde{\alpha}\left(\cdot\right); q\left(\cdot\right)\right) \quad \forall\, t \le T, \tag{4.12}$$

where $\tilde{q}_t = \tilde{q}$ is the initial distribution of the tracers, and $q(\cdot) := q_s(x), t \le s \le T$, indicates the dependence on the whole continuous curve. The following lemma can be found by comparing the solutions in the corresponding HJEs.

Lemma 4.3. *Given any $t \le T$ and $(q_s, \varphi_s), t \le s \le T$, to be the unique classical solutions of the MFG-2 model (3.5), the optimal solution $(\tilde{q}_s, \tilde{\phi}_s)$ of (4.11) with the optimal value function $\mathcal{U}(\tilde{q}, t; q(\cdot))$ exists uniquely and satisfies the following relation:*

$$\tilde{\phi}_s\left(x\right) = -\frac{\delta\tilde{\mathcal{U}}}{\delta\tilde{q}}\left(\tilde{q}_s, x, s; q\left(\cdot\right)\right) = \varphi_s\left(x\right). \tag{4.13}$$

Proof. Since φ_s is given by the optimal solution of the MFG-2 model, it satisfies the equation with the Hamiltonian (4.7)

$$\partial_s\varphi_s = -\frac{\delta\mathcal{H}_2}{\delta q}\left(q_s, \varphi_s\right) = -H_2\left(x, \nabla\varphi_s, q_s\right) - D\Delta\varphi_s + F\left(x, q_s\right) - \mathcal{T}^* \cdot \left(q_s \nabla\varphi_s\right).$$

Similarly, $\tilde{\phi}_s$ is the optimal solution of the problem (4.11), which satisfies the MFG-1 model with the new running cost $\tilde{F}$. Thus using the Hamiltonian (4.9) we have

$$\partial_s\tilde{\phi}_s = -\frac{\delta\tilde{\mathcal{H}}_2}{\delta\tilde{q}}\left(\tilde{q}_s, \tilde{\phi}_s; q_s, \varphi_s\right) = -H_1\left(x, \nabla\tilde{\phi}_s; q_s\right) - D\Delta\tilde{\phi}_s + \tilde{F}\left(x, q_s, \varphi_s\right).$$

Notice that by definition we have the identities $H_1(x,p;q) = H_2(x,p,q)$ and $\tilde{F}(x,q_s,\varphi_s) = F(x,q_s) - \mathcal{T}^* \cdot (q_s\nabla\varphi_s)$. In addition, $\varphi_T(x) = \tilde{\phi}_T(x) = -G(x,q_T)$ have the same terminal condition. Comparing the above two equations, we obtain $\tilde{\phi}_s = \varphi_s$ due to the uniqueness of solution to the HJE. And the first equality in (4.13) comes by Proposition 4.1. ∎

With this lemma, we can link the two sets of optimal solutions $(\tilde{q}_s, \tilde{\phi}_s)$ and (q_s, φ_s) from the MFG-1 and MFG-2 models accordingly as follows.

Theorem 4.4. *Given the solutions $(q_s, \varphi_s), t \le s \le T$, of the MFG-2 model (3.5), the optimal value function $\tilde{\mathcal{U}}(\tilde{q}, t)$ in (4.12) satisfies the following functional HJE:*

$$
\begin{aligned}
&\partial_t \tilde{\mathcal{U}}\left(\tilde{q},t\right)-\frac{1}{2}\int\left|\nabla\frac{\delta\tilde{\mathcal{U}}}{\delta\tilde{q}}\left(\tilde{q},x,t\right)\right|^2\tilde{q}\left(x\right)\mathrm{d}x+\int F\left(x,q_t\right)\tilde{q}\left(x\right)\mathrm{d}x\\
&\quad+\int\left[\tilde{q}\left(x\right)\mathcal{T}q_t\left(x\right)\cdot\nabla\frac{\delta\tilde{\mathcal{U}}}{\delta\tilde{q}}\left(\tilde{q},x,t\right)+q_t\left(x\right)\mathcal{T}\tilde{q}\left(x\right)\cdot\nabla\frac{\delta\tilde{\mathcal{U}}}{\delta\tilde{q}}\left(\tilde{q},x,t\right)\right]\mathrm{d}x\\
&\quad+D\int\left[\tilde{q}\left(x\right)\Delta\frac{\delta\tilde{\mathcal{U}}}{\delta\tilde{q}}\left(\tilde{q},x,t\right)\right]\mathrm{d}x=0,\qquad t\le T,\\
&\tilde{\mathcal{U}}\left(\tilde{q},T\right)=\int G(x,q_T)\tilde{q}\left(x\right)\mathrm{d}x.
\end{aligned}
\tag{4.14}
$$

Especially, with the same initial condition $\tilde{q}_t=q_t=q$, the modified MFG-1 model (4.11) will give the same optimal solution as the MFG-2 model (3.4),

$$
\tilde{q}_s\left(x\right)=q_s\left(x\right),\ \tilde{\phi}_s\left(x\right)=\varphi_s\left(x\right),\qquad \textit{for } t\le s\le T.
$$

Above, we suppressed the implicit dependence $\tilde{\mathcal{U}}(\tilde{q},s):=\tilde{\mathcal{U}}(\tilde{q},s;q(\cdot))$ on the entire curve $q(\cdot)$ for cleaner notation. Notice that the value function $\tilde{\mathcal{U}}$ defined in (4.12) is different from $\mathcal{V}$ in (3.4), while Theorem 4.4 says that we can recover the same optimal solution of the MFG-2 model by solving the easier noncoupled system (4.10).

Proof. From Proposition 4.1, we have using the new Hamiltonian (4.9)

$$
\begin{aligned}
\partial_t\tilde{\mathcal{U}}\left(\tilde{q},q,t\right)&=\tilde{\mathcal{H}}_2\left(\tilde{q},-\frac{\delta\tilde{\mathcal{U}}}{\delta\tilde{q}}\left(\tilde{q},x,t\right);q_t,\varphi_t\right)\\
&=\int\left[H_1\left(x,-\frac{\delta\tilde{\mathcal{U}}}{\delta\tilde{q}};q_t\right)-D\Delta\frac{\delta\tilde{\mathcal{U}}}{\delta\tilde{q}}-\tilde{F}\left(x,q_t,\varphi_t\right)\right]\tilde{q}\left(x\right)\mathrm{d}x.
\end{aligned}
$$

This gives the HJE (4.14) using the explicit expression for H_1 and $\varphi_t=-\frac{\delta\tilde{\mathcal{U}}}{\delta\tilde{q}}(\tilde{q}_t,x,t)$ from Lemma 4.3.

Next, since (q_s,φ_s), $s\le t\le T$, is given by the optimal solution of (4.6), we have

$$
\partial_s q_s=-\nabla\cdot\left[\left(\mathcal{T}q_s+\nabla\varphi_s\right)q_s\right]+D\Delta q_s=-\nabla\cdot\left[\left(\mathcal{T}q_s+\nabla\tilde{\phi}_s\right)q_s\right]+D\Delta q_s
$$

with $\tilde{\phi}_s=\varphi_s$, $s\le t\le T$, from Lemma 4.3. Then the identical solutions for $\tilde{q}_s$, q_s can be found directly by comparing with (4.10a) with the same initial value and by the uniqueness of the linear equation (4.10a). ∎

5. Computational strategies for the MFG models. With the explicit formulations for the MFG models, we develop practical computational algorithms for solving the MFG equations to find the optimal solution and control. Especially with the developed link between the MFG-1 and MFG-2 models, we can solve the coupled nonseparable MFG-2 system based on an iterative strategy using the modified form of the decoupled MFG-1 system (4.11).

5.1. Practical choices of the cost functions. We propose the cost (activation) functional to be optimized in the control problems in the following form:

$$\mathcal{G}(q_T) + \int_t^T \mathcal{L}(q_s, \alpha_s)\,\mathrm{d}s = \mathcal{G}(q_T) + \int_t^T \left[\int \tilde{L}(q_s, \alpha_s)\,\mathrm{d}x + \mathcal{F}(q_s)\right]\mathrm{d}s, \tag{5.1}$$

where $\mathcal{G}(q)$ quantifies the *terminal error* in the final target state and $\mathcal{L}(q,\alpha)$ is the *running loss* to characterize the cost along the control process, which is further decomposed to the cost on the control forcing $\tilde{L}$ and the cost on the running state $\mathcal{F}$. First, the control cost $\tilde{L}(q,\alpha)$ is set as

$$\tilde{L}(q,\alpha) = L(\alpha)q, \quad L(\alpha) = \frac{1}{2}|\alpha|^2. \tag{5.2}$$

The term regularizes the strength of the control effect α according to the flow measure q. In particular, in the region with a large value of q, a condensed particle concentration (in terms of probability measure) or a strongly turbulent fluid field (in terms of the flow vorticity) is implied. Thus the average kinetic cost for this region is the quadratic function of the control $|\alpha|^2$ weighted by the particle concentration q.

Specifically, the functional $\mathcal{F}(q)$ calibrates the energy fluctuations away from the initial and final states during the entire control process, and $\mathcal{G}(q)$ calibrates the difference at the final time step $t = T$. It is natural to require that the flow energy cannot deviate too much away from the starting initial state Q_i so that the level of turbulence is maintained at a controlled level, while it should also approach the final target state Q_f at a rapid rate. Therefore, we consider the following two common choices of functionals according to the initial and final states $Q_i(x)$ and $Q_f(x)$:

- *L_2-distance*: The cost functionals compute the mean square deviation from initial and final target state using the linear combination $q' = \gamma(q - Q_i) + (1-\gamma)(q - Q_f)$ with $0 \le \gamma \le 1$ and $u' = \mathcal{T}q'$, that is,

$$\mathcal{F}(q) = \frac{1}{2}\int |u'|^2\,\mathrm{d}x = \frac{1}{2}\int |\mathcal{T}q'|^2\,\mathrm{d}x \quad \text{with } F(q,x) := \frac{\delta \mathcal{F}}{\delta q} = \mathcal{T}^* \cdot \mathcal{T}q', \tag{5.3a}$$

$$\mathcal{G}(q_T) = \frac{1}{2}\int |q_T - Q_f|^2\,\mathrm{d}x \quad \text{with } G(q,x) := \frac{\delta \mathcal{G}}{\delta q} = q_T - Q_f. \tag{5.3b}$$

- *KL-divergence*: Since q can be viewed as the probability density of the Lagrangian tracer field, the cost functionals can compare the KL-divergence (relative entropy) with the distributions from the linear combination of the initial and final target states $\bar{Q} = \gamma Q_i + (1-\gamma)Q_f$ with $0 \le \gamma \le 1$, that is,

$$\mathcal{F}(q) = D_{\mathrm{KL}}(q, \bar{Q}) = \int q \log \frac{q}{\bar{Q}}\mathrm{d}x \text{ with } F(q,x) := \frac{\delta \mathcal{F}}{\delta q} = 1 + \log \frac{q}{\bar{Q}}, \tag{5.4a}$$

$$\mathcal{G}(q_T) = D_{\mathrm{KL}}(q_T, Q_f) = \int q_T \log \frac{q_T}{Q_f}\mathrm{d}x \text{ with } G(q,x) := \frac{\delta \mathcal{G}}{\delta q} = 1 + \log \frac{q_T}{Q_f}. \tag{5.4b}$$

5.2. Algorithms to solve the decoupled MFG-1 model. Here, we propose computational strategies to solve the MFG models (3.1) and (3.4). Equivalently, we can develop ensemble-based control strategies based on the stochastic control models (3.6) and (3.7). First, for the MFG-1 model (3.1), the optimal solution can be found by separately solving the decoupled forward and backward MFG equations (3.2).

Notice that above in solving the forward equation (3.2a), an alternative approach is to adopt the SDE formulation (3.6) to get the approximated optimal density solution ρ_s through an MC ensemble method. This approach could be advantageous in practical problems to efficiently recover the density distribution. Therefore, we can propose the ensemble-based algorithm corresponding to Algorithm 5.1.

At the limit $N \to \infty$, Algorithm 5.2 for finite ensemble approximation converges to the original Algorithm 5.1 at the continuum limit. This ensemble approach provides an effective alternative strategy to recover the target optimal tracer density without running the usually more expensive Fokker–Planck equation especially in the higher-dimensional cases. The ensemble approach will become more useful next for controlling the transition in flow states.

5.3. Iterative algorithm to solve the coupled MFG-2 model. Recall that the optimal solution for the MFG-2 model solves the coupled MFG-2 system (3.5). In solving the MFG-2 model (3.4), we need to deal with the coupled forward and backward equations (3.5) together. To address this difficulty, we first solve a separable MFG according to Algorithm 5.1 or 5.2. Then the optimal solution is achieved by an iterating approach as finding a fixed point.

We introduce a map $(\tilde{q}_s, \tilde{\alpha}_s) = \mathcal{P}(q_s, \alpha_s)$ defined as the solution of the modified MFG-1 model (4.10) with a given $\{q_s, \alpha_s\}, t \le s \le T$, i.e., $(\tilde{q}_s, \tilde{\alpha}_s)$ solves

Algorithm 5.1. MFG-1 model for optimal control of tracer field using PDE model.

Model setup: Given flow vorticity field $\{q_s\}_{t\le s\le T}$ and initial tracer density $\rho(x)$

1: solve the HJE (3.2b) backward in time to get the function $\phi_s(x)$ with $\phi_T(x) = -G(x, q_T)$ at $s = T$.
2: recover the control for the entire time window $\alpha_s(x) = \nabla\phi_s(x), t \le s \le T$.
3: solve the continuity equation (3.2a) forward in time using the optimal control $\alpha_s(x)$ to get the optimal tracer density starting from the initial configuration $\rho_t(x) = \rho(x)$.

Algorithm 5.2. MFG-1′ model for controlling tracer field using finite ensemble model.

Model setup: Given flow vorticity field $\{q_s\}_{t\le s\le T}$ and initial tracer density $\rho(x)$
Initial condition: generate random samples $X_t^i \sim \rho(x), i = 1, \ldots, N$, via $\rho(x)$.

1: solve the HJE (3.2b) backward in time to get the function $\phi_s(x)$ with $\phi_T(x) = -G(x, q_T)$ at $s = T$.
2: recover the control $\alpha_s(x) = \nabla\phi_s(x), t \le s \le T$, for the entire time window.
3: solve the SDE (3.6) forward in time independently for each sample trajectory $X_s^i, t \le s \le T$.
4: recover the optimal tracer density using the empirical distribution $\rho_s^N(x) = \frac{1}{N}\sum_i \delta_{X_s^i}(x)$.

$$\partial_s \tilde{q}_s + \nabla \cdot \left[\left(\mathcal{T} q_s + \nabla \tilde{\phi}_s \right) \tilde{q}_s \right] = D \Delta \tilde{q}_s, \tag{5.5a}$$

$$\partial_s \tilde{\phi}_s + \frac{1}{2} \left| \nabla \tilde{\phi}_s \right|^2 + \mathcal{T} q_s \cdot \nabla \tilde{\phi}_s + D \Delta \tilde{\phi}_s = F(x, q_s) - \mathcal{T}^* \cdot (q_s \alpha_s), \tag{5.5b}$$

with the initial and final conditions $\tilde{q}_t(x) = q(x)$ and $\tilde{\phi}_T(x) = -G(x, q_T)$, and the new control $\tilde{\alpha}_s = \nabla \tilde{\phi}_s$. The above equations (5.5) define a separable problem that is easy to solve individually. From Theorem 4.4, if we can find a fixed point of the map, $(q_s, \alpha_s) = \mathcal{P}(q_s, \alpha_s)$, based on the modified MFG-1 model (5.5), the fixed-point solution provides the solution for the MFG-2 system (3.4). Therefore, we expect the solution of (5.5) to give good approximation to the optimal solution of the MFG-2 model given a close estimate of the input states $\{q_s, \alpha_s\}$ (see Claim 5.1). If we further assume the solution of (3.5) is unique, we can solve the MFG-2 model through an iterative algorithm.

Based on the above consideration, we propose the following iterative strategy aiming to minimize the value function $\mathcal{I}(q_s, \alpha_s)$ of the MFG-2 model. Let $\{\tilde{q}_s^{(n+1)}, \tilde{\alpha}_s^{(n+1)}\}$ be the solution of (5.5) using the input functions $\{q_s^{(n)}, \alpha_s^{(n)}\}$ (from the previous iteration step). First, we construct a new state q_s^μ as the linear interpolation of the two functions

$$q_s^\mu = \mu q_s^{(n)} + (1 - \mu)\, \tilde{q}_s^{(n+1)} \tag{5.6}$$

with $0 \le \mu \le 1$. Then, the corresponding new interpolation state of α_s^μ is constructed based on the consistency with the continuity equation such that

$$\partial_s q_s^\mu + \nabla \cdot \left[\left(\mathcal{T} q_s^\mu + \alpha_s^\mu \right) q_s^\mu \right] = D \Delta q_s^\mu.$$

This can be achieved by comparing the equations for $\{\tilde{q}_s^{(n+1)}, \tilde{\alpha}_s^{(n+1)}\}$ and $\{q_s^{(n)}, \alpha_s^{(n)}\}$. The solution can be found to follow the relation

$$\alpha_s^\mu = \frac{\mu \alpha_s^{(n)} q_s^{(n)} + (1 - \mu)\, \tilde{\alpha}_s^{(n+1)} \tilde{q}_s^{(n+1)}}{\mu q_s^{(n)} + (1 - \mu)\, \tilde{q}_s^{(n+1)}} + (1 - \mu) \left(\mathcal{T} q_s^{(n)} - \mathcal{T} \tilde{q}_s^{(n+1)} \right). \tag{5.7}$$

Finally, the updated state is defined by the optimal μ at the point that minimizes the value of the cost function (3.4) of the MFG-2 model, that is,

$$q_s^{(n+1)} := q_s^{\mu^*},\ \alpha_s^{(n+1)} := \alpha_s^{\mu^*}, \quad \text{with } \mu^* = \operatorname*{argmin}_{0 \le \mu \le 1} \mathcal{I}\left(q_s^\mu, \alpha_s^\mu\right). \tag{5.8}$$

This finishes the one-step updating for the fixed-point iteration. We describe the algorithm using the iterative method to find the optimal control solution as follows.

A sufficient condition for the stability of the iterative scheme. In Algorithm 5.3, a critical step is taken to update the next stage solution using the optimal linear combination (5.6) instead of directly adopting the solution from (5.5). This is confirmed by the following necessary condition describing the stability of the iteration scheme.

Algorithm 5.3. MFG-2 model for optimal control of the flow field.

Initial condition: set up the initial flow vorticity $q_s^{(0)}$ and control functions $\alpha_s^{(0)}$.

1: **for** $n \le N_{\max}$ while $d(q_s^{(n)}, q_s^{(n-1)}) > \epsilon$ or $d(\alpha_s^{(n)}, \alpha_s^{(n-1)}) > \epsilon$ **do**

2: solve the separable equations (5.5) to get the new states $\{\tilde{q}_s^{(n+1)}, \tilde{\alpha}_s^{(n+1)}\}$ with input $\{q_s^{(n)}, \alpha_s^{(n)}\}$.

3: find the optimal μ^* that minimizes the cost function $\mathcal{I}(q_s^{\mu}, \alpha_s^{\mu})$ by line searching with a sequence of $\mu_i = \frac{i}{L}, i = 1, \ldots, L-1$, using the combination of the two states (5.6) and (5.7).

4: update the next states $q_s^{(n+1)} = q_s^{\mu^*}$ and $\alpha_s^{(n+1)} = \alpha_s^{\mu^*}$.

5: **end for**

Claim 5.1. *With the cost functions defined in* (5.3) *or* (5.4)*, the value of the target cost function in* (3.4) *is not guaranteed to decrease if the solution of* (5.5) *is directly applied to update the next stage. That is, we may have*

$$\mathcal{I}(\tilde{q}_s, \tilde{\alpha}_s) > \mathcal{I}(q_s, \alpha_s)$$

with $\mu = 0$ *during some iteration steps. On the other hand, one can expect to reduce the value of the cost function from the input* (q_s, α_s) *in every iteration,*

$$\mathcal{I}(q_s^{\mu}, \alpha_s^{\mu}) \le \mathcal{I}(q_s, \alpha_s), \tag{5.9}$$

by taking some $\mu > 0$ *in updating the solution in* (5.6).

Proof. Denote the value functional to be optimized above as

$$\mathcal{J}(\tilde{q}_s, \tilde{\alpha}_s; q_s, \alpha_s) = \int G(x, q_T)\tilde{q}_T(x)\,\mathrm{d}x + \int_t^T \int \left[L(\tilde{\alpha}_s) + \tilde{F}(x, q_s, \alpha_s)\right] \tilde{q}_s(x)\,\mathrm{d}x\mathrm{d}s.$$

First, since $(\tilde{q}_s, \tilde{\alpha}_s)$ is the optimal solution of the problem (4.11), they minimize the corresponding value function

$$\mathcal{J}(\tilde{q}_s, \tilde{\alpha}_s; q_s, \alpha_s) \le \mathcal{J}(q_s, \alpha_s; q_s, \alpha_s), \tag{5.10}$$

as long as we choose (q_s, α_s) also satisfying the continuity equation in (3.5a).

On the other hand, the target loss function to minimize has the form

$$\mathcal{I}(q_s, \alpha_s) = \mathcal{G}(q_T) + \int_t^T \left[\int L(\alpha_s) q_s(x)\,\mathrm{d}x + \mathcal{F}(q_s)\right] \mathrm{d}s.$$

To evaluate the effect from the one-step update, we define the improvement function

$$
\begin{aligned}
g(\mu) &= \mathcal{I}(q_s^\mu, \alpha_s^\mu) - \mathcal{I}(q_s, \alpha_s) \\
&\le \left[\mathcal{G}(q_T^\mu) - \int G(x, q_T)\tilde{q}_T\right] + \int_t^T \left[\mathcal{F}(q_s^\mu) - \int F(x, q_s)\,\tilde{q}_s\right] \mathrm{d}s \\
&\quad + \left[\int G(x, q_T) q_T - \mathcal{G}(q_T)\right] + \int_t^T \left[\int F(x, q_s)\, q_s - \mathcal{F}(q_s)\right] \mathrm{d}s \\
&\quad + \int \left[L(\alpha_s^\mu)\, q_s^\mu - L(\tilde{\alpha}_s)\,\tilde{q}_s\right] + \int_t^T \left[\int (q_s \alpha_s) \cdot \mathcal{T}(\tilde{q}_s - q_s)\right] \mathrm{d}s.
\end{aligned} \tag{5.11}
$$

Above in the inequality, (5.10) is used to link the solutions from the modified MFG-1 model (5.5) with the updated new state $q_s^\mu = \mu q_s + (1-\mu)\,\tilde{q}_s$.

First from (5.6) and (5.7) with $\mu = 1$, we have $q_s^\mu = q_s, \alpha_s^\mu = \alpha_s$, thus

$$
g(1) = \mathcal{I}(q_s, \alpha_s) - \mathcal{I}(q_s, \alpha_s) = 0.
$$

Then at the other end point with $\mu = 0$, that is, $q_s^\mu = \tilde{q}_s, \alpha_s^\mu = \tilde{\alpha}_s$, we can compute the explicit expressions for the right-hand side of (5.11) based on the explicit loss functions. Also since the terminal and running costs $\mathcal{G}$ and $\mathcal{F}$ share similar forms in both L_2 and KL-divergence cases, we compute the terminal cost below and the running cost will follow with very similar expressions. For the L_2 loss (5.3), we find

$$
\left[\mathcal{G}_{L_2}(\tilde{q}_T) - \int G_{L_2}(x, q_T)\tilde{q}_T\right] + \left[\int G_{L_2}(x, q_T) q_T - \mathcal{G}_{L_2}(q_T)\right] = \frac{1}{2}\int (\tilde{q}_T - q_T)^2 \ge 0,
$$

and for the KL-divergence loss (5.4)

$$
\left[\mathcal{G}_{KL}(\tilde{q}_T) - \int G_{KL}(x, q_T)\tilde{q}_T\right] + \left[\int G_{KL}(x, q_T) q_T - \mathcal{G}_{KL}(q_T)\right] = \int \tilde{q}_T \log \frac{\tilde{q}_T}{q_T} \ge 0.
$$

In the last line of (5.11), the first term will vanish at $\mu = 0$ since $q_s^0 = \tilde{q}_s, \alpha_s^0 = \tilde{\alpha}_s$. However, the sign of the second term with the integrand, $(q_s\alpha_s)\cdot\mathcal{T}(\tilde{q}_s - q_s)$, becomes indefinite and could frequently reach positive values during the iterations. Therefore, a positive value could be reached on the right-hand side of (5.11) using both loss functions. Thus, the total cost $\mathcal{I}$ is not guaranteed to decrease with direct update using a constant $\mu = 0$ (see Figure 3 as a confirmation from direct numerical results).

Finally, notice that using the specific loss functions (5.3) or (5.4), the function $g(\mu) = A\mu^2 + B\mu + C + O(\|\tilde{q}_s - q_s\|^2)$ can be expressed as a quadratic function about μ in the leading order expansion. Further, it can be checked that the coefficient before the μ^2 term is positive. Thus to ensure there exists some μ^* such that $g(\mu^*) < 0$, we only need to consider the case with $g(0) > 0$. In addition, taking into account $g(1) = 0$, the property of the quadratic function suggests that negative values of $g(\mu)$ will be reached with some $\mu > 0$ unless the single critical case with minimun reached at $\mu = 1$. ∎

6. Model performance using a prototype test model. In this section, we demonstrate the performance of the proposed MFG models through detailed numerical experiments. A prototype nonlinear advection-diffusion model modified from the viscous Burgers equation is used as a test example simulating multiscale vortical flows. This simple model preserves many key properties of more general turbulent models appearing in many fields, while providing a clean tractable setup for confirming the important basic properties discussed in the previous sections.

6.1. The modified Burgers equation as a prototype test model. In the numerical tests, we introduce the control problem for the modified viscous Burgers (MVB) equation

$$\partial_s q_s(x) + \nabla \cdot [u_s(x)\, q_s(x)] = \nu \Delta q_s(x) + f_s(x) \tag{6.1}$$

with the control forcing in the form $f_s = -\nabla \cdot (\alpha_s q_s)$. The solution is defined on the one- or two-dimensional periodic domain of size L. The vorticity field q_s can be projected on the Fourier modes; then the advection velocity field u_s can be expressed under the spectral representation based on each wavenumber $k = (k_x, k_y)^\intercal$ as

$$u_s(x) = \mathcal{T} q_s(x) = \sum_{|k|\neq 0} i|k|^{-2} (k_y, -k_x)^\intercal \hat{q}_k(s)\, e^{ikx} \quad \text{and } q_s(x) = \sum_k \hat{q}_k(s)\, e^{ikx}.$$

In the one-dimensional case, the velocity field reduces to the simpler form $u_s(x) = \sum_{k\neq 0} ik^{-1} \hat{q}_k(s) e^{ikx}$. In fact, it is direct to check that if $u_s(x)$ satisfies the solution of the viscous Burgers equation, $q_s = -\partial_x u_s$ gives the solution of (6.1). Therefore, a sequence of exact steady state solutions can be constructed for the MVB equation (6.1) based on the explicit analytic solutions u_s [5], i.e., with two parameters σ, a,

$$Q_{\sigma,a}(x) = 2\nu\sigma^2 \operatorname{sech}^2(\sigma|x-a|). \tag{6.2}$$

The steady solutions indicate the persistent coherent structures in general turbulent flow fields. Therefore, we design the control problem for recovering the optimal control forcing f_s during $s \in [0, T]$ driving between two steady solutions from $Q_i(x) = Q_{\sigma,-L/2}(x)$ to $Q_f(x) = Q_{\sigma,L/2}(x)$. The cost functionals in the optimal control adopt the two typical examples in (5.3) and (5.4). It shows that many representative features of general interest including multiscale turbulent behavior and extreme events [1, 36] can be generated in the simplified MVB model (6.1).

In the numerical experiments, the MVB equation is solved by a pseudospectral method with a Galerkin truncated spectral representation of $J = 256$ modes in both x and y directions. The finite truncation model is suitable for more general applications with explicit multiscale turbulent spectra. The equation is integrated in time by an explicit-implicit Runge–Kutta method with the implicit part only for the dissipation term. Model parameters in the numerical tests are listed in Table 1. A typical steady state solution of the MVB equation is plotted in Figure SM1 in the supplementary materials showing the typical coherent flow structure. In the following, we first consider the simpler one-dimensional case giving a detailed discussion on both the MFG-1 model (3.1) for the control of the transport of passive tracers and the performance of the iterative strategy solving the MFG-2 model (3.4) for the control of the flow vorticity equation. Then, the control performance of the control model on the more complex two-dimensional flow equations is tested.

Table 1

Parameters used for the MVB test model. The last three columns show control parameters for the initial and final target states using (6.2).

ν	L	J	Δt	T	γ	σ	a
0.5	10	256	1×10^{-3}	10	0.2	1	$\pm L/2$

6.2. MFG-1 model for tracer field control. First, we show the performance of the tracer control model in the one-dimensional case according to Algorithms 5.1 and 5.2. The advection flow solution u_t is generated by the steady state solution $Q_{1,0}(x)$ of (6.1). We set the tracer initial density as $Q_i(x) = Q_{1,-L/2}(x)$ and the final target density as $Q_f(x) = Q_{1,L/2}(x)$. Therefore, the tracer control problem asks to find the optimal control action that drives the tracers across the "barrier" set by the advection flow in the center of the domain. Both the L_2 cost (5.3) and the KL-divergence cost (5.4) are applied in optimizing the cost function (3.1).

6.2.1. Control of tracer density function with the PDE model. Following Algorithm 5.1 for the MFG-1 model, we first find the control action $\alpha_s = \partial_x \phi_s$ by solving the decoupled backward equation (3.2b) using the prescribed solution of q_s, using the corresponding costs F and G from (5.3) or (5.4). Next, we solve the forward equation (3.2a) to get the controlled tracer density field using the achieved optimal control solution ϕ_s. The solution gives the optimal controlled tracer density field ρ_s together with the optimal control forcing α_s exerted on top of the transporting flow velocity $u_s = \mathcal{T} q_s$.

The optimal solutions for the MFG-1 model achieved with both L_2 and KL-divergence cost functions are plotted in Figure 1. Comparable control solutions are found under the different forms of cost functions. In this control problem for tracer density, the initial tracer field concentrates on the left side of the domain at $-L/2 = -5$ while the target field lies on the right at $L/2 = 5$. With the steady advection flow field u_s as shown in Figure SM1, the passive tracers are driven toward the center of the domain at $x = 0$. The control forcing is required to guide the tracers going against the tendency from the advection flow velocity. As a result, the controlled tracer field ρ_s diverged into two routes in opposite directions, one traveling across the center region of the domain and the other going across the boundary exploiting the periodic boundary condition, converging at the final target location. A strong control forcing α_s is exerted at the starting time to drive the tracer density quickly toward the target, then is reduced to smaller values to balance the running cost part of the control. The tracer density fields finally reach the target state ρ_T with good agreement, indicating successful control performance in both cases under different losses.

6.2.2. Control of empirical ensemble distributions with the SDE model. Correspondingly, we can use the ensemble SDE approach for solving the controlled optimal tracer density through estimating the empirical measure from the samples. Especially, Algorithm 5.2 for the tracer control model provides an effective way to generate samples agreeing with any non-Gaussian PDFs by setting it as the targeting state $X_T^i \sim Q_f$ for the terminal tracer density. Here, the initial MC samples of the tracers $X_0^i \sim \rho_0 = \mathcal{N}(\mu_0, \sigma_0^2)$ can be easily sampled from a normal distribution. The optimal control forcing α_s is still solved from the backward HJE (3.2b) with the terminal condition G defined by the target state Q_f. But instead, the

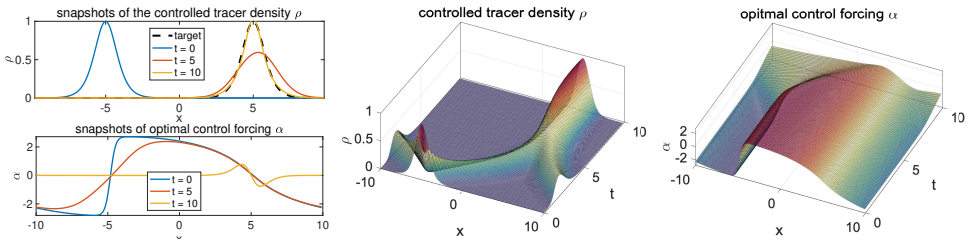

(a) L_2 loss

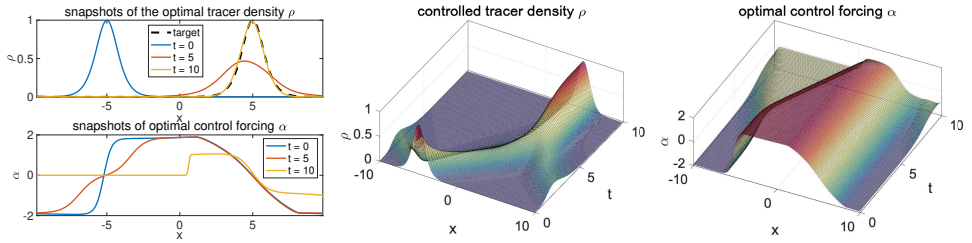

(b) KL-divergence loss

Figure 1. *Optimally controlled solutions of the MFG-1 model for tracer transport with L_2 and KL-divergence loss functions.*

Table 2

Mean square errors of the ensemble approximation of the target PDF (6.2) with different sample sizes.

N	500	1000	5000	10000
$\sigma = 0.5$	2.1×10^{-2}	6.6×10^{-3}	1.2×10^{-3}	7.3×10^{-4}
$\sigma = 1$	5.8×10^{-3}	5.1×10^{-3}	1.1×10^{-3}	8.6×10^{-4}

forward continuity equation is solved by the MC approximation of the SDE (3.6). Therefore, the resulting ensemble members through the controlled SDE model sample the target PDF, $\frac{1}{N}\sum_i \delta_{X_T^i} \simeq Q_f$. This method will become more useful for sampling high-dimensional PDFs including highly non-Gaussian structures.

In Figure 2, we show one simple test to sample non-Gaussian PDFs in the shape of the functions (6.2). We run the SDE model with a relatively large ensemble of $N = 1 \times 10^4$ samples. The ensemble size will be sufficient as long as it captures the main shapes of the PDFs. The accuracy using different sample sizes is listed in Table 2, and the errors mostly happen in the tail region where a smaller number of particles are used. The initial samples are drawn from a standard normal distribution. Two target PDFs with linear tails of different extents $\sigma = 0.5$, $\sigma = 1$ are used. It shows that the final empirical sample distributions of the tracer particles accurately capture the non-Gaussian shapes in the PDFs, which also agree with the PDE control model results. Deviation only appears in the long tail region due to insufficient representation of the extreme events. The ensemble representations will also be applied next using the SDE model for controlling flow vorticity states.

6.3. MFG-2 model for flow field control. Next, we test the one-dimensional flow control problem formulated by the MFG-2 model. In this case, we need to solve the coupled joint equations (3.5). Different from the previous tracer control problem, the continuity equation

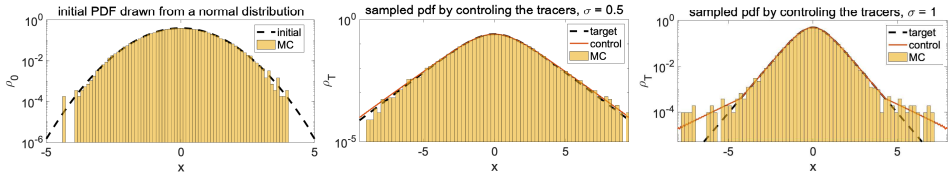

Figure 2. *Sampling non-Gaussian PDFs by controlling tracer density. Solid red lines show the results from the PDE control model, and the MC approach using the SDE model is shown in the yellow bars from the histogram.*

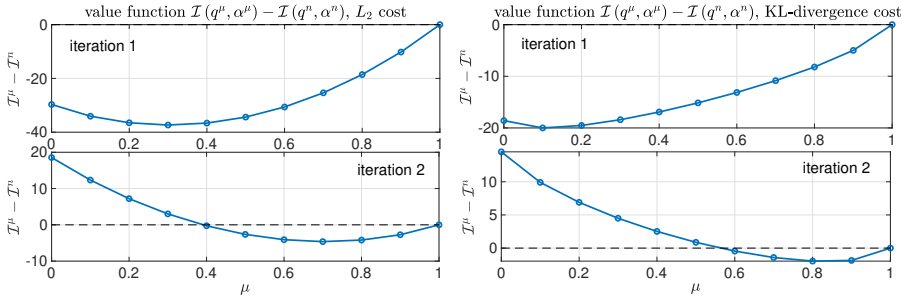

Figure 3. *Improvement in the target value function $\mathcal{I}(q_s^\mu,\alpha_s^\mu)-\mathcal{I}(q_s^n,\alpha_s^n)$ with different values of μ during the first two iterations using L_2 and KL-divergence cost.*

for q_s becomes nonlinear due to the explicit coupling with the advection velocity $u_s = \mathcal{T} q_s$. The forward and backward equations become closely coupled. The new iterative approach in Algorithm 5.3 is applied to solve the corresponding decoupled solution $\{\tilde{q}_s, \tilde{\varphi}_s\}$ from (5.5) using the solution $\{q_s^{(n)}, \varphi_s^{(n)}\}$ from the previous iteration step to find the converged optimal solution.

6.3.1. Effective updating strategy during iterations. We first confirm the necessary condition in Claim 5.1 for stable converging iterations. The initial states for $\{q_s^{(0)}, \varphi_s^{(0)}\}$ in the iterative algorithm are computed by solving the tracer control problem. The interpolated new state $q^\mu = \mu q^n + (1-\mu)\tilde{q}$ is required to be updated using the optimal combination parameter $\mu \neq 0$. In Figure 3, we plot the improvement in minimizing the value function $\mathcal{I}(q^\mu, \alpha^\mu) - \mathcal{I}(q^{(n)}, \alpha^{(n)})$ under the L_2 and KL-divergence cost during the first two iteration steps. Consistent with our analysis, the cost $\mathcal{I}(\tilde{q}_s, \tilde{\alpha}_s)$ as a function of μ gives approximately a quadratic structure with 0 at the right end $\mu = 1$ and indefinite values on the left $\mu = 0$. The cost function value by directly using the decoupled model solution $\{\tilde{q}_s, \tilde{\varphi}_s\}$ is indicated at $\mu = 0$. The direct solution is not guaranteed to reduce the target cost function from each step of the iteration. This confirms the inherent obstacle due to the instability in the iteration scheme especially during the initial iteration steps with larger errors. On the other hand, an improvement with negative values can always be achieved through a direct line search of the optimal μ to minimize the cost. Furthermore, it shows that the choice of the optimal μ can also effectively accelerate the convergence demanding only a few iteration steps.

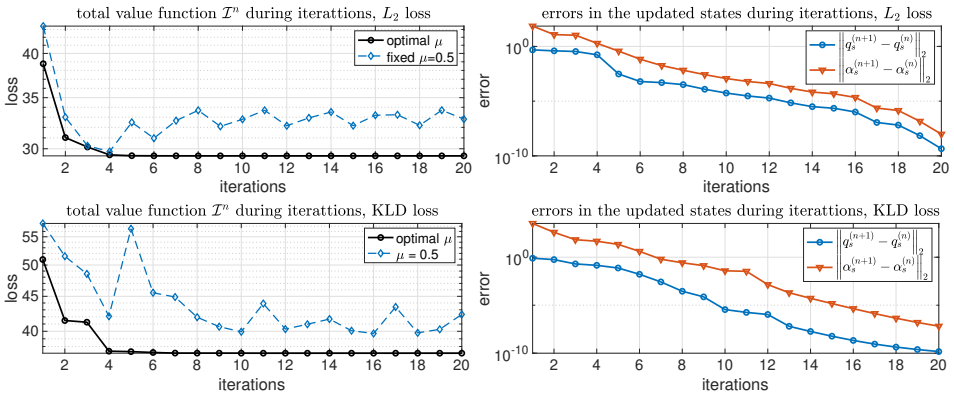

Figure 4. *Total value function $\mathcal{I}^n = \mathcal{I}(q_s^{(n)}, \alpha_s^{(n)})$ and the errors in the updated states $\{q_s^{(n)}, \alpha_s^{(n)}\}$ during the updating iterations using both L_2 and KL-divergence loss.*

As a more detailed illustration of the error development during iterations, Figure 4 plots the value function $\mathcal{I}(q_s^{(n)}, \alpha_s^{(n)})$ as well as the L_2 errors in both states $q_s^{(n)}, \alpha_s^{(n)}$. Each iteration update solves the separable forward and backward equations (5.5), and the computation time is just several seconds using a laptop computer. It shows that the value function decreases rapidly to its minimum value within a few iterations (~ 5 under both L_2 and KL-divergence loss). In comparison, we also plot the evolution of the loss function values using a fixed $\mu = 0.5$. Then, the value function cannot be minimized due to the frequent violation of the decreasing condition. This confirms the necessity of taking the adaptive choice of the combination parameter μ to reach the target fixed-point solution in the proposed iterative algorithm. We continue running the iterations further to longer than necessary steps. It shows that the errors in the target states keep decreasing to the refined optimal solution during the continuing iterations. This again confirms the stability of the proposed method.

6.3.2. Control performance with different cost functions. Here, we show the optimally controlled solutions achieved from the iterative algorithm. The final converged optimal solutions using both L_2 and KL-divergence loss functions are displayed in Figure 5. The controlled trajectories for q_s show a similar structure as in the tracer control case, while they are through completely different dynamical equations. This can be seen by the very different structures in the optimal control solutions of α_s. In fact, the solution illustrates the optimal route of transition between the two steady states of the flow solutions under the loss function.

Equivalently, we can solve the flow control problem using the SDE formulation (3.9) with a finite number of samples as described in the last formulation in section 3. In this approach, instead of solving the continuous forward equation for q_s we run an ensemble simulation for the Lagrangian tracers

$$\mathrm{d}X_s^i = \left[\mathcal{T} q_s^N\left(X_s^i\right) + \alpha_s^N\left(X_s^i\right)\right]\mathrm{d}s + \sqrt{2D}\mathrm{d}W_s^i$$

with $i = 1, \ldots, N$. Notice that the N samples are linked together by the empirical recovery of the flow field from the samples $q_s^N(x) = \frac{1}{N}\sum_{i=1}^N \delta_{X_s^i}(x)$. The optimal control α_s^N is solved through the backward HJE also using the empirical estimate q_s^N. The initial samples agreeing with the initial state Q_i are drawn by the strategy introduced in section 6.2.2.

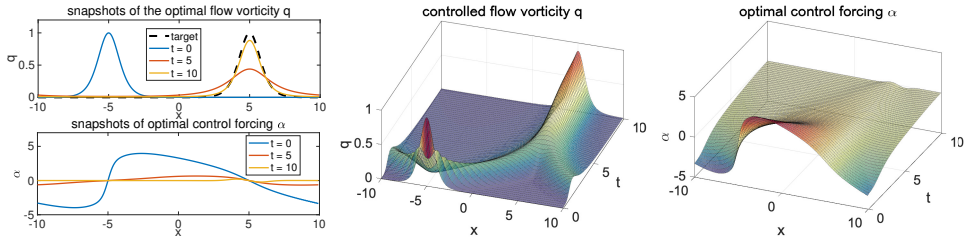

(a) L_2 loss

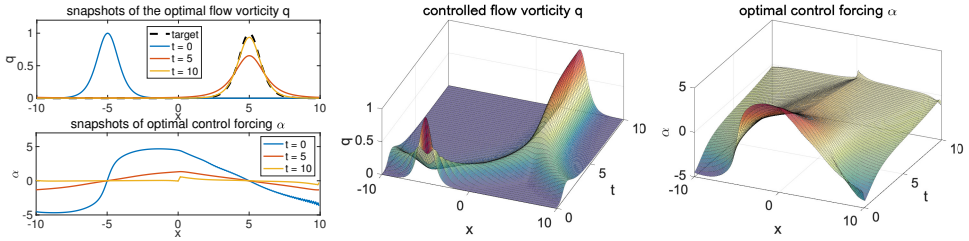

(b) KL-divergence loss

Figure 5. *Optimally controlled solution of MFG-2 model for vorticity transport with different loss functions.*

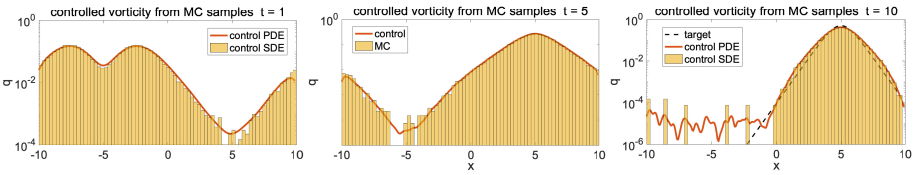

Figure 6. *Evolution of the controlled vorticity state q_t from the SDE model using the KL-divergence loss function.*

The ensemble-based particle approach becomes very useful in the generalization to higher-dimensional cases where solving the forward Fokker–Planck PDE using finite difference or finite element methods becomes highly expensive. Figure 6 illustrates the controlled solutions using the KL-divergence loss at several time instants from the SDE model using $N = 1 \times 10^4$ samples. The corresponding optimal PDE solution in Figure 5 is compared on top of the SDE solution from the empirical distribution. Good agreements are observed in the two equivalent approaches indicating effective skill in the control methods. In addition, a more detailed comparison of the optimal value function $\mathcal{V}(q,t)$ from different initial state $q = Q_{\sigma,-L/2}$ and starting time t is shown in Figure SM2 in the supplementary materials, where the optimal solutions go through a relatively similar transient stage to reach the final target state.

6.4. MFG models for controlling two-dimensional flows. Finally, we test the performance of the MFG models on controlling the two-dimensional flow fields. The same algorithm is applied to solving the corresponding two-dimensional MVB equation (6.1) in the same fashion. In this case, the equation becomes the diffusive transport of the vorticity field q_s. The same steady solutions as in (6.2) are taken as the initial and final target states centered at $(-L/2, -L/2)$ and $(L/2, L/2)$, respectively. The same set of parameters is applied

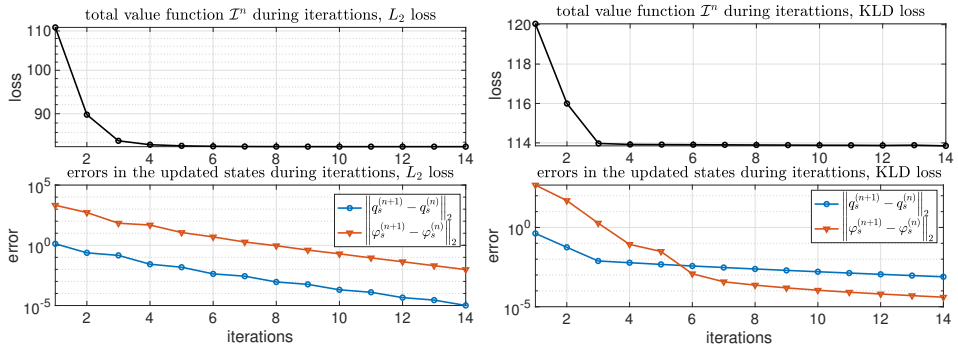

Figure 7. *Total value function $\mathcal{I}^n = \mathcal{I}(q_s^{(n)}, \alpha_s^{(n)})$ and errors in the updated states $\{q_s^{(n)}, \varphi_s^{(n)}\}$ during updating iterations using both L_2 and KL-divergence loss in the two-dimensional flow.*

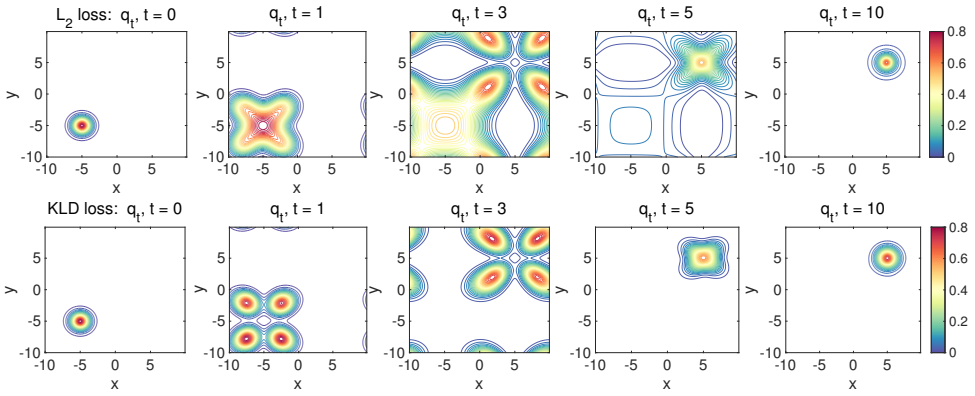

Figure 8. *Optimal controlled solutions q_s in the two-dimensional control problem at several time instants t under both the L_2 and KL-divergence loss functions.*

in the two-dimensional flow control test, and the same loss functions (5.3) and (5.4) are used measuring the errors in the two-dimensional functions. Following the same strategy as in the one-dimensional tests, we first apply Algorithm 5.1 to get the initial guess $q_s^{(0)}, \varphi_s^{(0)}$. Then the optimal control solution is achieved by the iterative strategy in Algorithm 5.3.

The value function as well as the errors during each iteration are plotted in Figure 7. Still, we run a larger number of iterations to illustrate the evolution of the errors. As in the one-dimensional case, the loss value quickly converges to the minimum value after only a few iterations under both cost functions. The fast convergence is especially important in the two-dimensional case due to the much higher computational cost. The errors in the states $q_s^{(n)}$ and $\varphi_s^{(n)}$ also quickly drop to small values implying fast convergence and keep decreasing with more iterations just refining the detailed structures of the final solution. The optimal trajectories for the optimal solution q_s are shown in Figure 8 as well as the corresponding control φ_s in Figure SM3 in the supplementary materials. It is observed that the optimal control forcing successfully moves the flow vorticity from the initial state to its final target. One interesting observation in the two-dimensional case is that the controlled flow solution demonstrates different routes to the target under the L_2 and KL-divergence loss functions.

Under the L_2 loss, the solution goes through a gradual transition with decaying value in the initial state. On the other hand, under the KL-divergence loss, the initial density is moved directly to the final target along the four symmetric directions with the doubly periodic boundary. Further investigation is needed for a complete understanding of the distinctive behaviors under different loss functions.

7. Summary. We proposed MFG models for controlling the nonlinear transport of tracer densities and flow vorticity fields under a unified mathematical framework. The main results are summarized in the following new developments:

- Two MFG models (MFG-1 and MFG-2) are designed for controlling the passive tracer density and flow vorticity field.
- Equivalent stochastic formulations are derived by tracking Lagrangian tracers/particles immersed in the advected flow field as interacting players.
- The corresponding functional HJEs for the value functions are also derived in both the noncoupled tracer control and the coupled flow control problems.
- A link is built between the tracer and flow control models as well as their optimal value functions showing an interesting connection between the two proposed MFG models with a nonseparable Hamiltonian.
- Effective iterative algorithms are proposed for solving the MFG model as coupled forward and backward equations in the flow control problem.

The performance of the proposed MFG models and algorithms is tested on the MVB equation displaying representative multiscaled and nonlinear dynamics. Fast convergence and effective control performance are demonstrated in both the one- and two-dimensional test cases and under loss functions in different metrics. For future research, more detailed convergence analysis about the iterative scheme is to be developed quantifying the approximation error and convergence rate of the new methods. It is also interesting to compare the performance of related methods such as proposed in [30, 17]. In practical applications of the idealized mathematical models, a closer link needs to be built in modeling the macroscopic flow dynamics and the controlled motion of microscopic fluid particles. We plan to design efficient ensemble methods using the proposed numerical algorithms and develop suitable strategies adaptive to more general high-dimensional multiscale complex fluid systems such as soft matter and plasma flows [15, 16, 22].

REFERENCES

[1] R. V. Abramov, G. Kovačič, and A. J. Majda, *Hamiltonian structure and statistically relevant conserved quantities for the truncated Burgers-Hopf equation*, Comm. Pure Appl. Math., 56 (2003), pp. 1–46, https://doi.org/10.1002/cpa.3032.

[2] Y. Achdou and I. Capuzzo-Dolcetta, *Mean field games: Numerical methods*, SIAM J. Numer. Anal., 48 (2010), pp. 1136–1162, https://doi.org/10.1137/090758477.

[3] Y. Achdou, P. Cardaliaguet, F. Delarue, A. Porretta, and F. Santambrogio, *Mean Field Games*, Lecture Notes in Math. 2281, Springer, Cham, 2021.

[4] B. D. Anderson and J. B. Moore, *Optimal Control: Linear Quadratic Methods*, Courier, North Chelmsford, MA, 2007.

[5] A. Boritchev, *Decaying turbulence in the generalised Burgers equation*, Arch. Ration. Mech. Anal., 214 (2014), pp. 331–357, https://doi.org/10.1007/s00205-014-0766-5.

[6] S. L. Brunton and B. R. Noack, *Closed-loop turbulence control: Progress and challenges*, Appl. Mech. Rev., 67 (2015), 050801, https://doi.org/10.1115/1.4031175.
[7] P. Cardaliaguet, F. Delarue, J.-M. Lasry, and P.-L. Lions, *The Master Equation and the Convergence Problem in Mean Field Games*, Princeton University Press, Princeton, NJ, 2019.
[8] P. Cardaliaguet and S. Hadikhanloo, *Learning in mean field games: The fictitious play*, ESAIM Control Optim. Calc. Var., 23 (2017), pp. 569–591, https://doi.org/10.1051/cocv/2016004.
[9] E. Carlini and F. J. Silva, *A fully discrete semi-Lagrangian scheme for a first order mean field game problem*, SIAM J. Numer. Anal., 52 (2014), pp. 45–67, https://doi.org/10.1137/120902987.
[10] R. Carmona and F. Delarue, *Probabilistic Theory of Mean Field Games with Applications*, Vols. I and II, Springer, Cham, 2018.
[11] A. Chambolle and T. Pock, *A first-order primal-dual algorithm for convex problems with applications to imaging*, J. Math. Imaging Vis., 40 (2011), pp. 120–145, https://doi.org/10.1007/s10851-010-0251-1.
[12] O. Guéant, J.-M. Lasry, and P.-L. Lions, *Mean field games and applications*, in Paris-Princeton Lectures on Mathematical Finance 2010, Lecture Notes in Mathematics 2003, Springer, Berlin, Heidelberg, pp. 205–266, https://doi.org/10.1007/978-3-642-14660-2_3.
[13] J. Covington, D. Qi, and N. Chen, *Effective statistical control strategies for complex turbulent dynamical systems*, Proc. A, 479 (2023), 20230546, https://doi.org/10.1098/rspa.2023.0546.
[14] P. H. Diamond, S. Itoh, K. Itoh, and T. Hahm, *Zonal flows in plasma—A review*, Plasma Phys. Control. Fusion, 47 (2005), pp. R35–R161, https://doi.org/10.1088/0741-3335/47/5/R01.
[15] P. H. Diamond, S.-I. Itoh, and K. Itoh, *Modern Plasma Physics*, Cambridge University Press, Cambridge, UK, 2010, https://doi.org/10.1017/CBO9780511780875.
[16] M. Doi, *Soft Matter Physics*, Oxford University Press, New York, 2013.
[17] G. Fu, H. Ji, W. Pazner, and W. Li, *Mean field control of droplet dynamics with high-order finite-element computations*, J. Fluid Mech., 999 (2024), https://doi.org/10.1017/jfm.2024.983.
[18] W. Gangbo, A. R. Mészáros, C. Mou, and J. Zhang, *Mean field games master equations with nonseparable Hamiltonians and displacement monotonicity*, Ann. Probab., 50 (2022), pp. 2178–2217, https://doi.org/10.1214/22-AOP1580.
[19] Y. Gao, T. Li, X. Li, and J.-G. Liu, *Transition path theory for Langevin dynamics on manifolds: Optimal control and data-driven solver*, Multiscale Model. Simul., 21 (2023), pp. 1–33, https://doi.org/10.1137/21M1437883.
[20] Y. Gao, J.-G. Liu, and W. Li, *Master equations for finite state mean field games with nonlinear activations*, Discrete Contin. Dynam. Syst. Ser. B, 29 (2024), pp. 2837–2879, https://doi.org/10.3934/dcdsb.2023204.
[21] V. J. García-Garrido and S. Wiggins, *Lagrangian descriptors and the action integral of classical mechanics*, Phys. D, 434 (2022), 133206, https://doi.org/10.1016/j.physd.2022.133206.
[22] M.-H. Giga, A. Kirshtein, and C. Liu, *Variational modeling and complex fluids*, in Handbook of Mathematical Analysis in Mechanics of Viscous Fluids, 2017, Springer, Cham, pp. 1–41.
[23] O. Guéant, *Mean field games equations with quadratic Hamiltonian: A specific approach*, Math. Models Methods Appl. Sci., 22 (2012), 1250022, https://doi.org/10.1142/S0218202512500224.
[24] M. Huang, R. P. Malhamé, and P. E. Caines, *Large population stochastic dynamic games: Closed-loop McKean–Vlasov systems and the Nash certainty equivalence principle*, Commun. Inf. Syst., 6 (2006), pp. 221–252, http://dx.doi.org/10.4310/CIS.2006.v6.n3.a5.
[25] D. Inoue, Y. Ito, T. Kashiwabara, N. Saito, and H. Yoshida, *A fictitious-play finite-difference method for linearly solvable mean field games*, ESAIM Math. Model. Numer. Anal., 57 (2023), pp. 1863–1892, https://doi.org/10.1051/m2an/2023026.
[26] J. Kim and T. R. Bewley, *A linear systems approach to flow control*, Annu. Rev. Fluid Mech., 39 (2007), pp. 383–417, https://doi.org/10.1146/annurev.fluid.39.050905.110153.
[27] P. Kooloth, D. Sondak, and L. M. Smith, *Coherent solutions and transition to turbulence in two-dimensional Rayleigh-Bénard convection*, Phys. Rev. Fluids, 6 (2021), 013501, https://doi.org/10.1103/PhysRevFluids.6.013501.
[28] J.-M. Lasry and P.-L. Lions, *Mean field games*, Jpn. J. Math., 2 (2007), pp. 229–260, https://doi.org/10.1007/s11537-007-0657-8.

[29] M. Lauriere, *Numerical methods for mean field games and mean field type control*, in Mean Field Games, Proc. Sympos. Appl. Math. 78, AMS, Providence, RI, 2021, pp. 221–282, https://doi.org/10.1090/psapm/078/06.
[30] W. Li, W. Lee, and S. Osher, *Computational mean-field information dynamics associated with reaction-diffusion equations*, J. Comput. Phys., 466 (2022), 111409, https://doi.org/10.1016/j.jcp.2022.111409.
[31] W. Li, S. Liu, and S. Osher, *Controlling conservation laws* II*: Compressible Navier-Stokes equations*, J. Comput. Phys., 463 (2022), 111264, https://doi.org/10.1016/j.jcp.2022.111264.
[32] D. G. MacMartin, B. Kravitz, D. W. Keith, and A. Jarvis, *Dynamics of the coupled human-climate system resulting from closed-loop control of solar geoengineering*, Clim. Dynam., 43 (2014), pp. 243–258, https://doi.org/10.1007/s00382-013-1822-9.
[33] A. J. Majda, *Introduction to PDEs and Waves for the Atmosphere and Ocean*, Courant Lect. Notes Math. 9, AMS, Providence, RI, 2003.
[34] A. J. Majda and P. R. Kramer, *Simplified models for turbulent diffusion: Theory, numerical modelling, and physical phenomena*, Phys. Rep., 314 (1999), pp. 237–574, https://doi.org/10.1016/S0370-1573(98)00083-0.
[35] A. J. Majda and D. Qi, *Effective control of complex turbulent dynamical systems through statistical functionals*, Proc. Natl. Acad. Sci. USA, 114 (2017), pp. 5571–5576, https://doi.org/10.1073/pnas.1704013114.
[36] A. J. Majda and I. Timofeyev, *Remarkable statistical behavior for truncated Burgers-Hopf dynamics*, Proc. Natl. Acad. Sci. USA, 97 (2000), pp. 12413–12417, https://doi.org/10.1073/pnas.230433997.
[37] H. P. McKean, Jr., *A class of Markov processes associated with nonlinear parabolic equations*, Proc. Natl. Acad. Sci. USA, 56 (1966), pp. 1907–1911, https://doi.org/10.1073/pnas.56.6.1907.
[38] J. Pedlosky, *Geophysical Fluid Dynamics*, Springer, Cham, 2013.
[39] D. Qi and A. J. Majda, *Predicting extreme events for passive scalar turbulence in two-layer baroclinic flows through reduced-order stochastic models*, Commun. Math. Sci., 16 (2018), pp. 17–51, https://doi.org/10.4310/CMS.2018.v16.n1.a2.
[40] D. Qi and A. J. Majda, *Rigorous statistical bounds in uncertainty quantification for one-layer turbulent geophysical flows*, J. Nonlinear Sci., 28 (2018), pp. 1709–1761, https://doi.org/10.1007/s00332-018-9462-1.
[41] D. Qi and A. J. Majda, *Transient metastability and selective decay for the coherent zonal structures in plasma drift wave turbulence*, J. Nonlinear Sci., 29 (2019), pp. 2297–2339, https://doi.org/10.1007/s00332-019-09544-5.
[42] B. J. Zhang and M. A. Katsoulakis, *A Mean-Field Games Laboratory for Generative Modeling*, preprint, arXiv:2304.13534, 2023.